Mechanical Analysis of the 44.5 mm bore Nb$_3$Sn Dipole Magnet[*]

Deepak R. Chichili

Technical Division / Engineering and Fabrication Department
Fermilab, Batavia, IL 60510

1.0   Introduction

A 1 m long dipole model with a nominal field of 11-12 T based on Nb$_3$Sn technology is being developed at Fermilab in collaboration with LBNL and KEK. The design consists of a two layer shell-type coil with a 44.5 mm of bore and cold iron yoke. Before getting into the details of the present mechanical design a brief summary of various approaches taken by different laboratories to support the coil structure is presented.

1.1   D20 by LBNL

The mechanical support structure for D-20 consisted of stainless steel collars with 9 mm thickness, iron yoke, an aluminum spacer and stainless steel shell. Both the straight section and the ends were collared and the prestress due to collaring was about 15 MPa. A vertically split yoke with a tapered gap and a Al spacer with 0.25 mm clearance was used. This clearance allows the compression of the collar and the coils to reach the design prestress after assembly (i.e., after welding the skin onto the yoke assembly). The design coil prestress was 110 MPa for inner layer and 90 MPa for outer layer. The yoke gap was designed to be closed (due to shrinkage of aluminum spacer) after cooldown to increase the stiffness of the whole mechanical structure.

1.2   Nb$_3$Sn Dipole Magnet by CERN-ELIN

The mechanical design consisted of collars made up of a special aluminum alloy surrounded by two vertically split iron halves and a outer retaining cylinder also made of a special aluminum alloy. A "hybrid" mechanical structure was used in which the coil/collar assembly at room temperature provides only a part of the final coil pre-stress. During cool down, the coil/collar assembly is further compressed due to the shrinkage of the outer aluminum cylinder by closing the vertical gap between the split iron halves.

1.3   Nb$_3$Sn Dipole Magnet by Univ. of Twente

Ring shaped shrink fitted aluminum collaring system was used for controlled room temperature prestress and for better bending stiffness. A separate stainless steel pole inserts allows shrinking of these collars around the coils, thus increasing the pre-stress in the coils during cool down. A vertically split iron was used with the split open during all stages. The yoke assembly was contained in a stainless steel cylinder.

---

[*] Several variations of the Fermilab design have been analyzed. This report presents some of these and the reader is referred to the technical note by G. Ambrosio for the rest of them.

Both D20 and the magnet built at CERN rely on precise gap dimensions between the yoke halves. This is necessary to increase the stiffness of the structure so that the coil assembly remains under compression during excitation. This problem was overcome at University of Twente by using a shrink fit aluminum collar. However this design is not a practical approach for long accelerator magnets. Thus the goal for the Fermilab design was to have a mechanical support structure which is easy to assemble and more forgiving on the tolerances of yoke gap dimensions and should be able to extend to long accelerator magnets. Further we decided that the pre-stress levels in coils should not exceed 100 to 120 MPa at all stages of the magnet to decrease the amount of degradation in the conductor.

2.0   Fermilab Design

Fig. 1 shows the schematic of the Fermilab design. The mechanical support structure consists of a spacer, a vertically split iron yoke, clamp and stainless steel skin. Note that the yoke gap will remain open at all stages of the magnet. This was chosen to eliminate the requirement of precise gap dimensions. The spacer will be aligned with respect to the coil assembly using pole extensions and the yoke will be aligned with the spacer only at the mid-plane (since the yoke gap will remain open). Some unique features of the present design are as follows:

- The inner coil will be first wound and cured at 120-150 $^{\circ}$C for 30 mins and then the outer coil will be wound on top of the inner coil and this assembly will be cured again. At the end of this step we get one half of the coil assembly which has been formed into right shape and size. This coil assembly will be easy to handle as it is almost a solid structure. Note that this procedure is similar to NbTi coil technology.

- Each half of the coils will then be assembled together before reaction. The entire coil assembly will then be reacted and impregnated resulting in a cylinder or pipe consisting of coils, pole inserts and ground insulation. The advantage in following this procedure is that the entire assembly (which involves lot of handling) will be done before reaction thus reducing the risk of damaging the superconductor.

The spacer and the yoke halves will be installed next. Then the yoke assembly will be compressed to the right dimensions to insert the clamp. Finally the whole assembly will welded using stainless steel shells. Magnet mechanics can be described briefly as follows

Yoking and Skinning

- Coil assembly along with the oversized spacers are compressed by the two yoke halves as the clamps are inserted. The length of the clamp is slightly smaller than the slot in the yoke to introduce a interference between the clamp and the yoke thus producing some pre-stress in the coil assembly.
- Skin halves are welded together further increasing the pre-stress in the coil assembly due to weld shrinkage.

Cooldown

- Aluminum spacer and the clamp contracts and compress the coil.
- Skin stress increases as it contracts more than the iron yoke.

These two factors result in increasing the coil pre-stress to the desired value.

Excitation

- Azimuthal Lorentz forces decrease the coil preload at the pole region; however because of the large pre-stress, coil remains in contact with the pole.
- Majority of the radial Lorentz forces act at the mid-plane thus increasing the stress in the coils. These forces are transmitted to the spacer, yoke and the skin.

The following table gives the basic parameters of the Fermilab design:

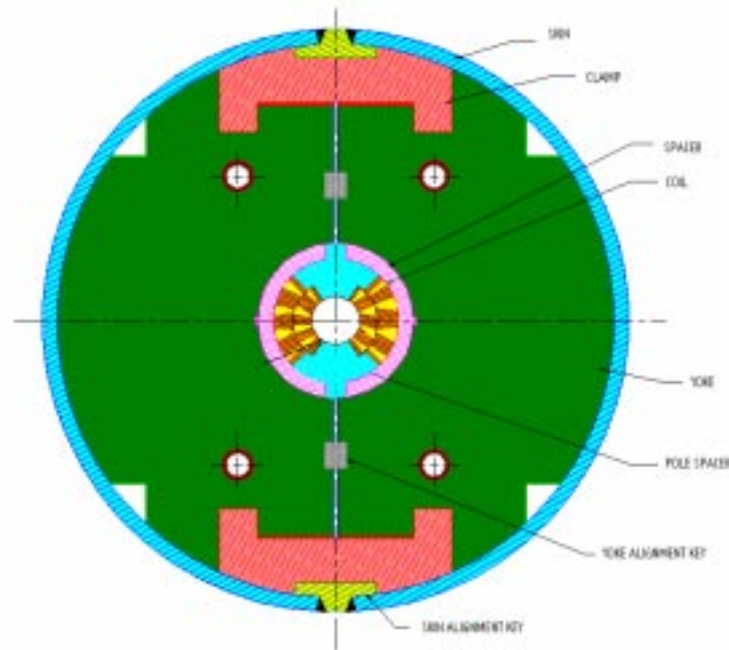| Parameter	Value	Cable	Value	Pressure @ 11T	
Bore Diameter (mm)	44.5	Number of strands	28	Azimuthal in mid-plane (MPa)	
Number of Layers	2	Strand diameter (mm)	1.012	inner	68.38
Number of blocks	6	Inner thickness (mm)	1.687	outer	72.15
- inner	3	Outer thickness (mm)	1.913	Radial in mid-plane (MPa)	
- outer	3	Width (mm)	14.232	inner	65.98
Number of turns	54	Insulation(mm)	0.125	outer	14.79

Figure 1: *Schematic of the Fermilab design (drawing courtesy of T. Arkan).*

3.0   Mechanical Analysis: Version - 1

Different variations of the design shown in Fig. 1 were analyzed. The variations include whether to obtain the required pre-stress using only the clamp or with clamp and skin acting as structural elements and with yoke gap remain open at all stages or open at room temperature and closed during cool down. Further the choice of spacer and clamp materials include aluminum and stainless steel.

The original idea was to obtain the required pre-stress with only the clamp acting as structural element and with yoke gap open. This choice would be an ideal scenario but the mechanical support structure was found to be not stiff enough to handle the excitation forces. Analysis showed that the iron yoke deflected more in the mid-plane as it is supported only by the clamp at the top thus loosing all the prestress in the coil. Hence the clamp only choice with yoke gap open was discarded. The other choice could be to use only clamp but have the yoke gap closed during cool down and remain closed during excitation to increase the stiffness of the overall support structure. This requires precise gap dimensions and hence we did not pursue this path. The rest of the analysis will be the with both clamp and skin acting as structural elements and with yoke gap open at all stages of the magnet.

Fig. 2 shows the ANSYS model used for the analysis. Quarter symmetry is used to reduce model size and model solution time. The surfaces between inner and outer coils and with the pole are glued in accordance with the proposed magnet fabrication sequence in which we intend to fabricate a "pipe". Frictional contact elements (CONTAC48) were used between the inner radius of the spacer and the outer ground insulation, between the outer radius of the spacer and the inner radius of the yoke and between outer radius of the yoke and the skin. Azimuthal interference between the spacer and the pole extension and interference between clamp and the yoke was obtained through COMBIN40 elements. The weld shrinkage is modeled by applying a displacement to the skin at room temperature. The following table lists the thermo-mechanical properties of the different materials used in the model:

Material	E (300 K) GPa	E (4.2 K) GPa	Poisson's ratio	Thermal Contraction K^{-1}
Coil	38	38	0.33	1.21×10^{-5}
Ground Insulation	14	14	0.3	2.58×10^{-5}
Copper (pole)	120	150	0.3	1.128×10^{-5}
Bronze	108	113	0.3	1.21×10^{-5}
Aluminum	70	81.6	0.3	1.47×10^{-5}
Iron	210	225	0.3	0.70×10^{-5}
S. S Steel	210	225	0.3	1.027×10^{-5}

Table 1: *Thermo-Mechanical properties of the materials used in the model.*

The inner radius of the spacer is 52.6 mm and the outer radius is 60 mm. The outer radius of yoke is 200 mm and the thickness of the skin is 8 mm. The length of the clamp is 50 mm and the width and height is 25 mm. The width of the pole extension is about 3 mm.
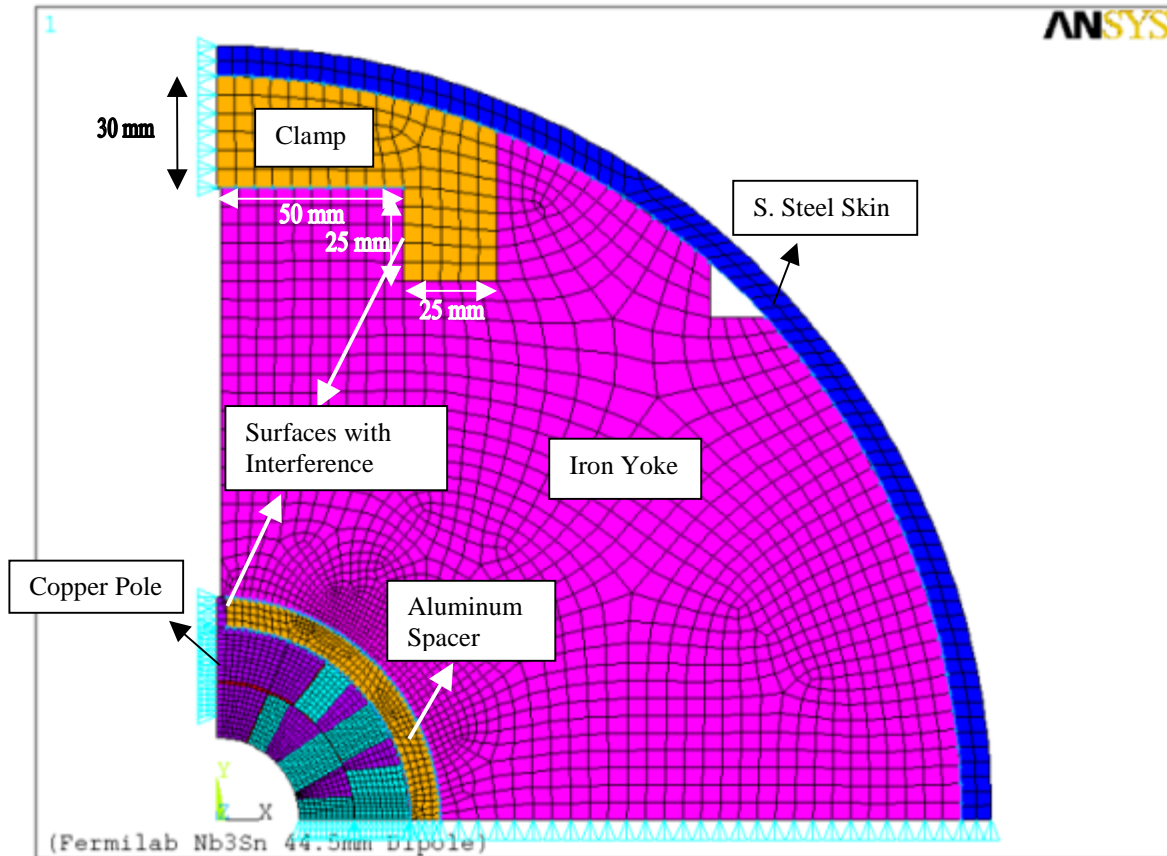

Figure 2: *ANSYS model.*

To simulate the cut in the pole the symmetry boundary conditions were removed (see Fig. 2). The purpose of this cut is to avoid excessive stress in the coils near the pole region during cooldown. This method used to model the cut will result in a stress concentration at the element where the boundary conditions were removed. In practice there will a fillet radius at this section to avoid this stress concentration.

Once it was decided that both clamp and skin will act as structural elements, the next step was is to find a scheme to apply right amount of pre-stress to the coils at room temperature so that that coils remain under compression during excitation. The first proposal was to store the strain energy in the aluminum spacer at room temperature thus loading the coils to a very low pre-stress. The idea is to then transfer this energy to the coil assembly during cooldown as aluminum spacer contracts more than the coil assembly. Analysis showed that this idea does not work as the differential thermal contraction between the aluminum spacer and the coil is too small. The following section

goes through this analysis in more detail as it might be useful in future if we some how reduce the thermal contraction coefficient of the coil.

Case 1: Low Prestress at Room Temperature

Parametric analysis was carried out by varying the thermal contraction coefficient of the coils from 0.5 to 4 µm/mm (from 293 K to 4.2 K) and keeping everything else constant. The azimuthal stress distribution in the coils at the room temperature is shown in Fig. 3. This stress distribution does not change with thermal contraction coefficient of the coils. Figs. 4(a) and 4(b) show the azimuthal stress distribution in the coils after cooldown with the thermal contraction coefficient of 3.5 and 1.5 µm/mm respectively. Note that with α = 1.5 µm/mm there is significant increase in the stress, however for α = 3.5 µm/mm, there is just rearrangement in stress distribution with mid-plane loosing the entire pre-stress.
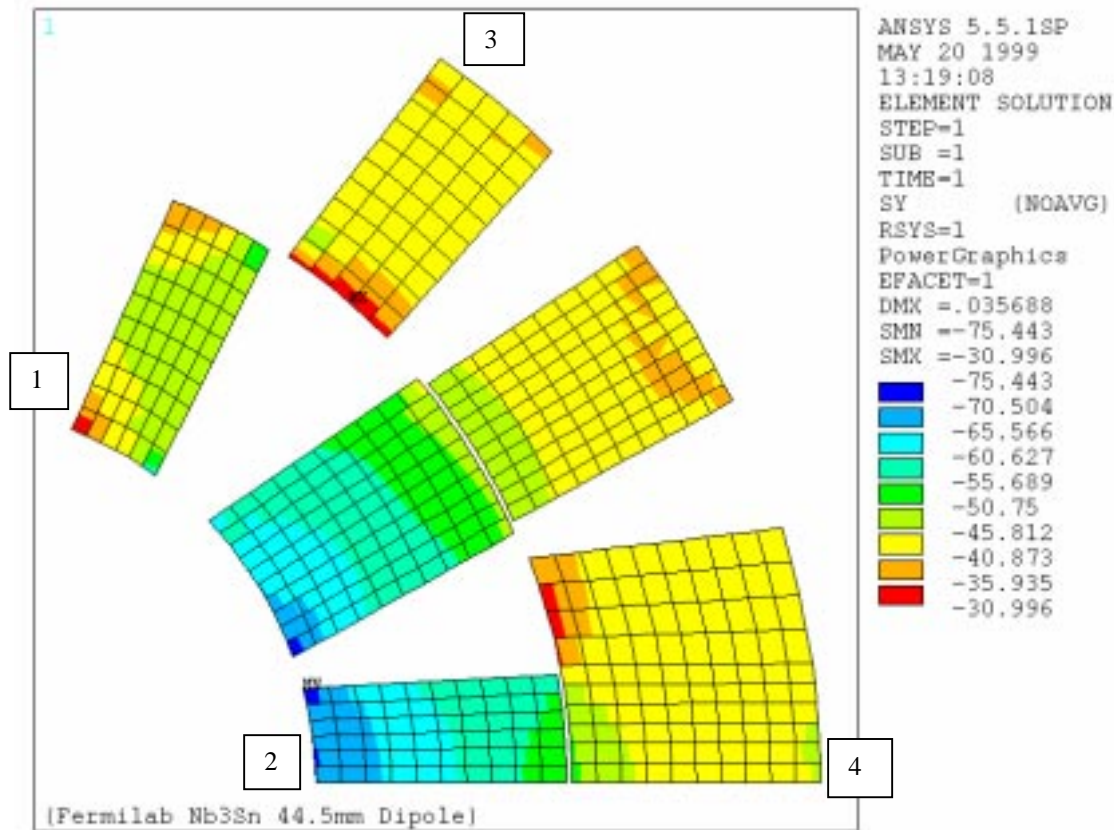

Figure 3: *Azimuthal stress distribution at room temperature.*

Fig. 5 shows the change in the coil azimuthal stress at positions 1 and 2 as shown in Fig. 3 for various thermal contraction coefficients. It is clear from the graph that as the thermal contraction of the coil approaches that of spacer the increase in the stress due to cooldown decreases. Similarly the drop in the azimuthal stress in the spacer decreases as the thermal contraction of the coils increases.
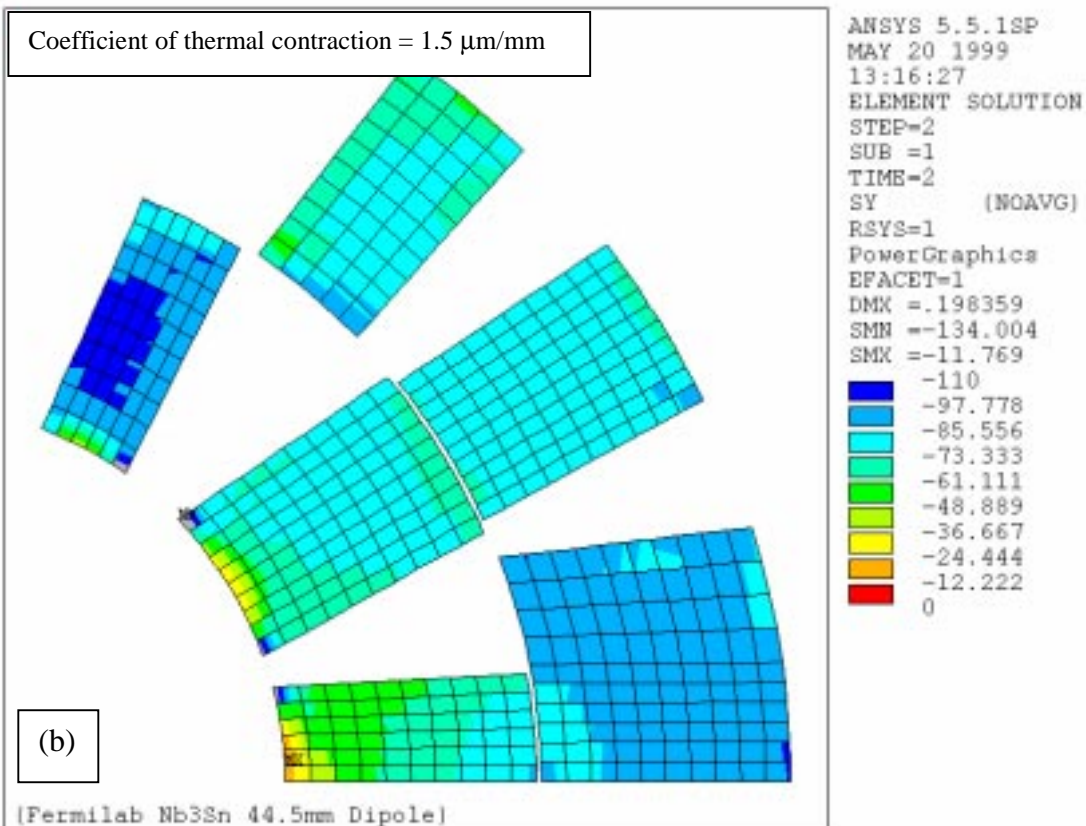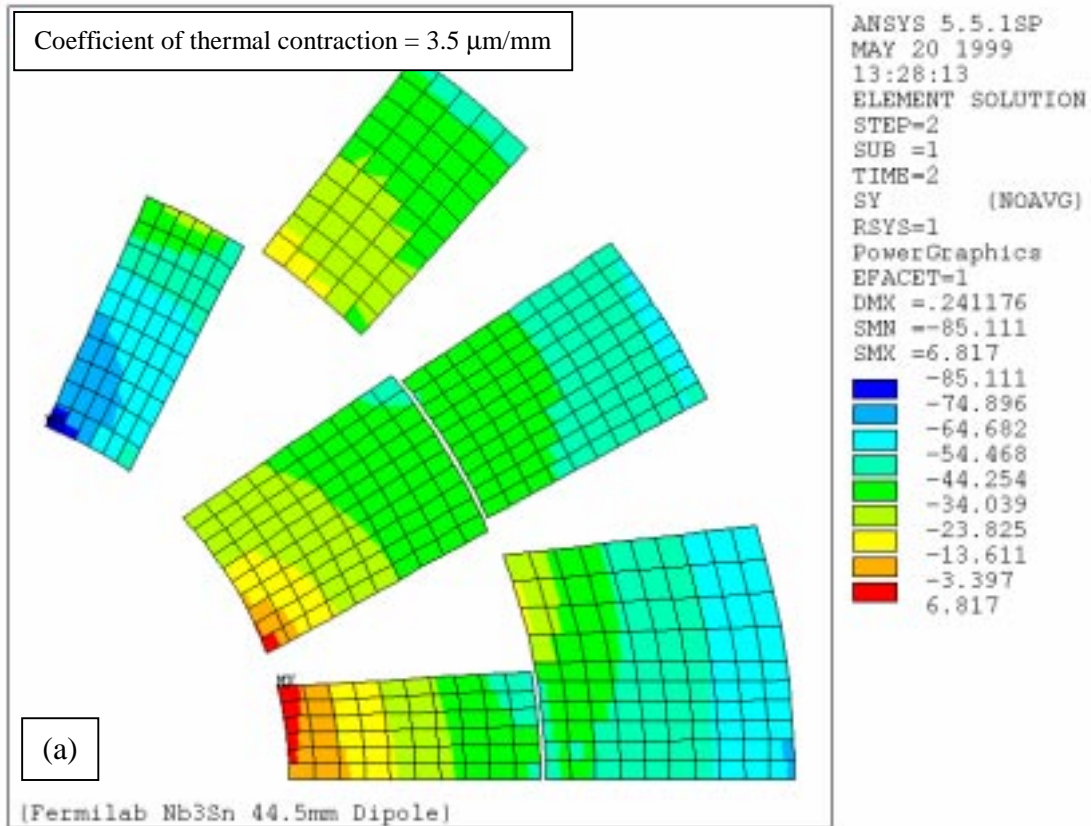
Coefficient of thermal contraction = 3.5 μm/mm

ANSYS 5.5.1SP
MAY 20 1999
13:28:13
ELEMENT SOLUTION
STEP=2
SUB =1
TIME=2
SY   (NOAVG)
RSYS=1
PowerGraphics
EFACET=1
DMX =.241176
SMN =-85.111
SMX =6.817

-85.111
-74.896
-64.682
-54.468
-44.254
-34.039
-23.825
-13.611
-3.397
6.817

(a)

[Fermilab Nb3Sn 44.5mm Dipole]

Coefficient of thermal contraction = 1.5 μm/mm

ANSYS 5.5.1SP
MAY 20 1999
13:16:27
ELEMENT SOLUTION
STEP=2
SUB =1
TIME=2
SY   (NOAVG)
RSYS=1
PowerGraphics
EFACET=1
DMX =.198359
SMN =-134.004
SMX =-11.769

-110
-97.778
-85.556
-73.333
-61.111
-48.889
-36.667
-24.444
-12.222
0

(b)

[Fermilab Nb3Sn 44.5mm Dipole]

Figure 4: *Azimuthal stress distribution in the coils after cool down.*
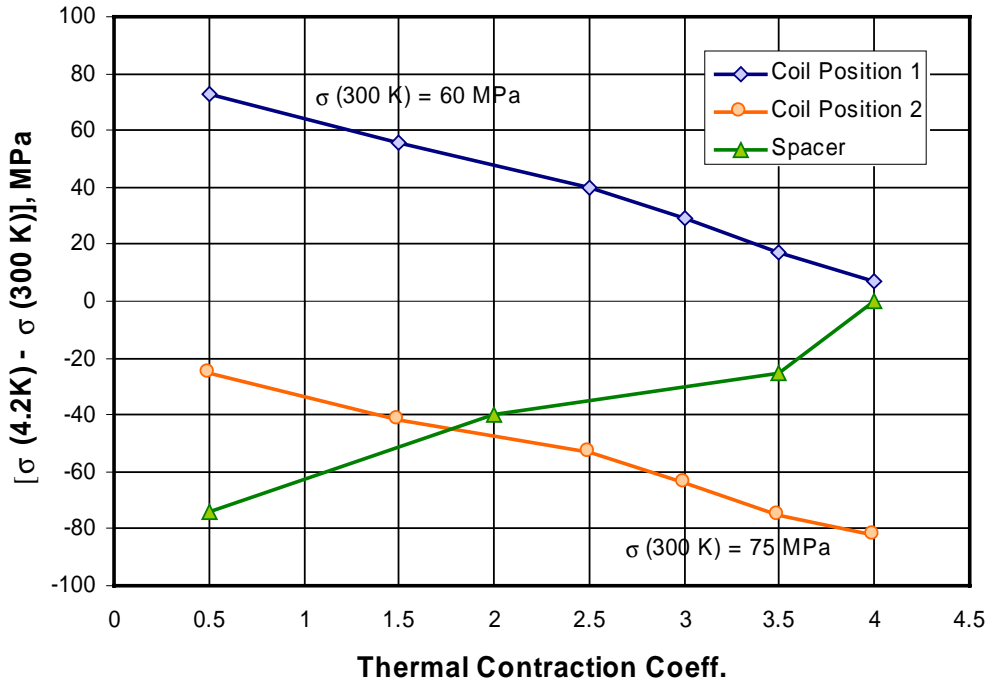
Figure 5: *Variation of the azimuthal stress in the coils due to cooldown with different thermal contraction coefficients.*

Thus the idea that we could transfer the stored strain energy in the spacer at room temperature to the coils after cooldown was discarded as the thermal contraction coefficient of the impregnated coils was measured to be 3.49 μm/mm from 300 to 4.2 K. Note that α = 4.25 μm/mm for aluminum. The next couple of sections outlines the procedure we could use to achieve the required pre-stress in the coils.

CASE 2: Aluminum Spacer and S. Steel Clamp

The spacer material is chosen as aluminum and that of the clamp as stainless steel. The results discussed in this section are with the azimuthal interference of 150 μm between the spacer and the pole extension, clamp / yoke interference of 350 μm and weld shrinkage of 0.4 mm. Fig. 6 shows the coil azimuthal stress distribution at room temperature, cooldown and at excitation. Note that 11 T is the design field and 12 T is the maximum field in the present magnet design. The stress distribution at room temperature is quite non uniform with maximum at the mid-plane and minimum at the pole region. The parameters are chosen to achieve such distribution at room temperature because on cooldown, the stress decreases at the mid-plane and increases at the pole due to boundary conditions and differential thermal contraction between various materials. Further having the maximum pre-stress at the pole region helps during excitation as the maximum azimuthal Lorentz forces are acting in this region, which reduces the pre-stress. However at the mid-plane, the radial forces increases the pre-stress during excitation. Note that at

12 T a very small portion of the coil (half the width of the cable) at the pole region looses all the pre-load. However the same section of the coil near the aperture is still under compression.

Table 2 lists the stresses (both azimuthal and radial) in various components of the magnet. Note that the maximum stress in the coil is less than 120 MPa at all stages of the magnet. The skin yields at room temperature; this can be useful as the jump in the coil stress will be much smaller beyond this point. The azimuthal stress in the spacer drops from 230 MPa at room temperature to 200 MPa at 4.2 K. It decreases further during excitation. But the spacer is always under compression and remain the contact with coil assembly on the inner radius and the yoke on the outer radius at all stages of the magnet.

Fig. 7 shows the radial displacement contours at room temperature, cooldown and at excitation. Note that at room temperature and at excitation, the radial deformation is quite uniform in the sense that the deformation at the pole region is same as that at mid-plane. However at 4.2 K, the radius at mid-plane is smaller that at pole region by about 80 μm.

	Azimuthal Stress, MPa				Radial Stress, MPa			
	300 K	**4.2 K**	**11 T**	**12 T**	**300 K**	**4.2 K**	**11 T**	**12 T**
COIL								
Position 1	70	119	13	4 / -9	0	5	0	-2
Position 2	106	26	100	110	0	5	0	-2
Position 3	75	78	36	40	37	41	27	30
Position 4	82	100	104	110	48	53	84	91
SPACER	233	200	177	155	60	71	90	90
σ_{coil}(**max**)	110	120	107	107	=Von-mises stress			
CLAMP	300	200	222	222	=Von-mises stress			
SKIN	250	350	350	355	=Von-mises stress			
δR	0	-81	0	0	=R(mid-Plane)-R (pole); μm			

Table 2: *Stresses in the various components of the magnet. Note that the positive values for azimuthal and radial stresses means compression.*

CASE 3: Aluminum Spacer and Aluminum Clamp

CASE 2 was repeated this time with aluminum clamp. Fig. 8 shows the azimuthal stress distribution in the coils at room temperature, cooldown and at excitation. The only difference being at room temperature, the azimuthal stress in the coils is lower in CASE 3 than in CASE 2, as the aluminum clamp deforms more than the stainless steel clamp. This also reduces the stress both in the spacer and skin at room temperature. However the stress distribution after cooldown and at 11 T is almost identical to CASE 2. The stresses in the various components of the magnet are shown in Table 3. Note that the maximum stress in the coils is about 115 MPa after cooldown.

	Azimuthal Stress, MPa				Radial Stress, MPa			
	300 K	4.2 K	11 T	12 T	300 K	4.2 K	11 T	12 T
COIL								
Position 1	67	116	11	2 / -12	0	0	4	0
Position 2	83	26	90	97	0	0	4	0
Position 3	62	78	33	42	33	40	27	28
Position 4	67	100	100	97	38	46	85	91
SPACER	175	150	167	160	60	71	90	90
CLAMP	117	104	104	140	=Von-mises stress			
SKIN	195	308	313	335	=Von-mises stress			
δR	3	-80	0	28	=R(mid-Plane)-R (pole); μm			

Table 3: *Stresses in the various components in the magnet for CASE 3.*

CASE 4: Aluminum Spacer and S. Steel Clamp with Vacuum Pipe

One of the ideas was to leave a very thin pipe (0.5 mm thick) attached to the inner bore of the magnet after impregnation. This makes the impregnation process much simpler as we have to remove only the inside mandrel which is attached to the pipe and not to the coil assembly. However this might pose a problem if we decide to have a cut in the pole. So this option is still being studied interms of magnet fabrication. However the analysis shows that this is infact a viable option. The stresses in the coils are slightly lower than CASE 2 (which was obtained without the vacuum pipe). The vacuum pipe decreases the peak stresses at the inner bore of the magnet thus reducing the stresses in the coil assembly by about 10% compared to CASE 2. Table 4 list the stresses in the coil assembly. Further the shear stresses near the vacuum pipe are less than 30 MPa.

	Azimuthal Stress, MPa				Radial Stress, MPa			
	300 K	4.2 K	11 T	12 T	300 K	4.2 K	11 T	12 T
COIL								
Position 1	47	98	11	-11	1	6	0	-3
Position 2	90	21	68	78	13	13	23	25
Position 3	74	81	45	40	42	40	33	36
Position 4	80	98	103	104	48	46	84	90
δR	0	-80	0	0	=R(mid-Plane)-R (pole); μm			

Table 4: *Stresses in the coil assembly for CASE 4.*

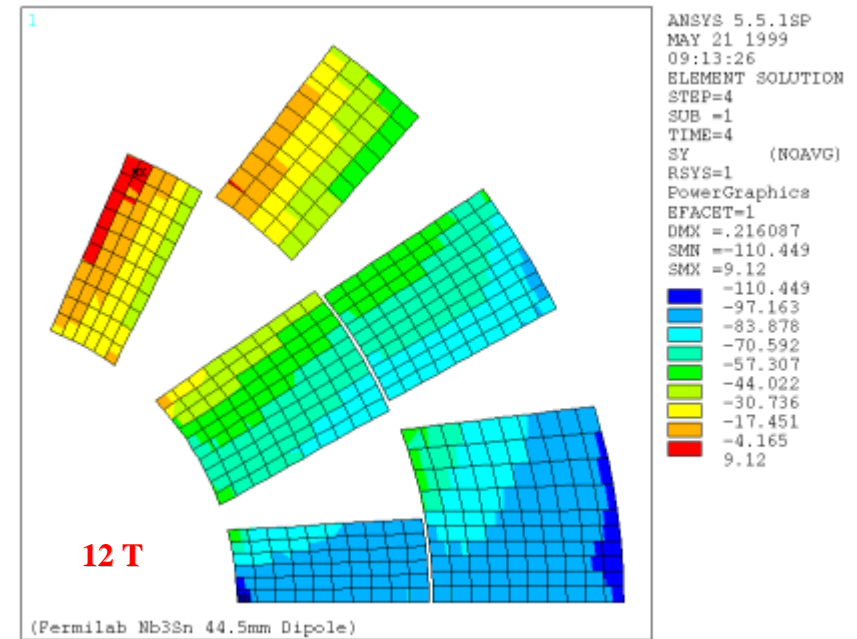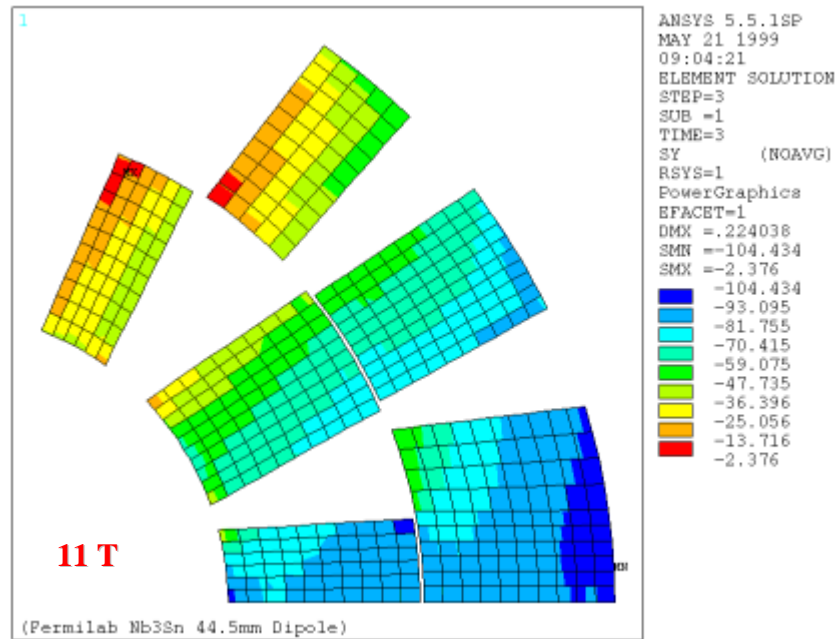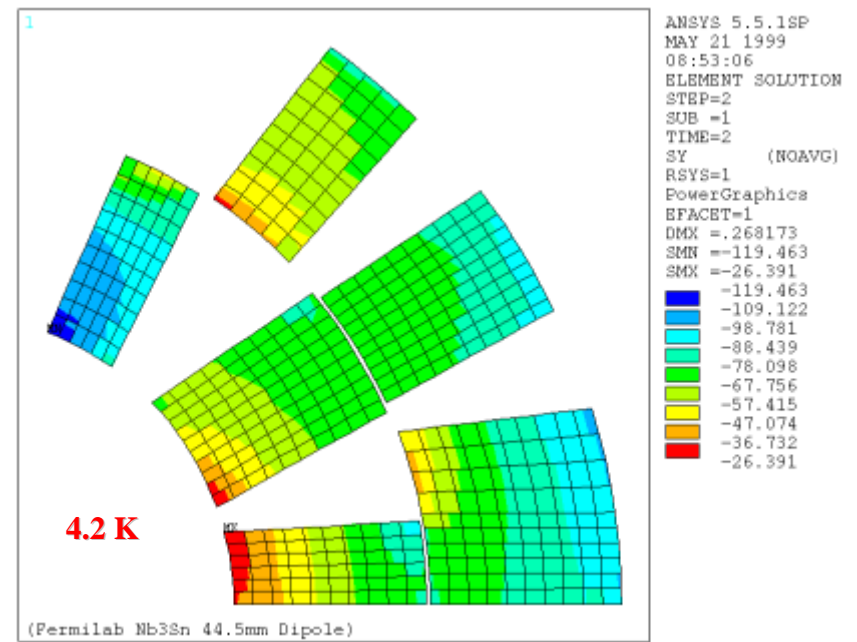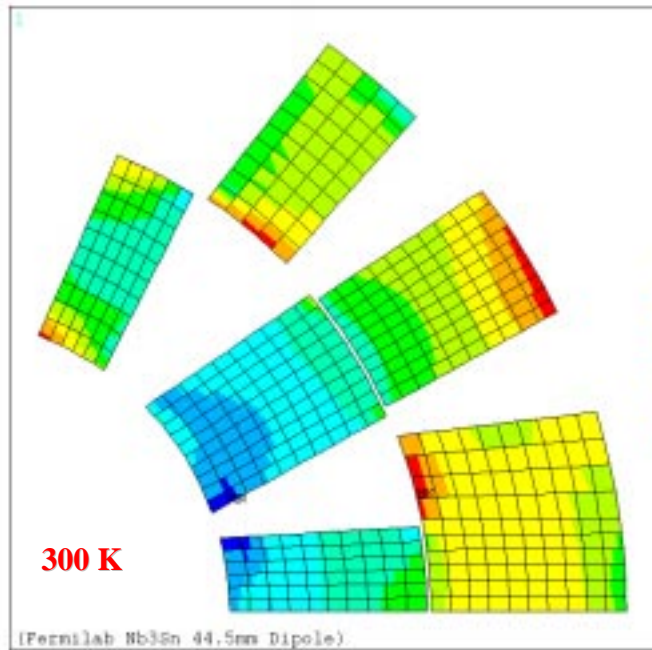**Figure 6**: *Azimuthal stress distribution in the coils for CASE 2*

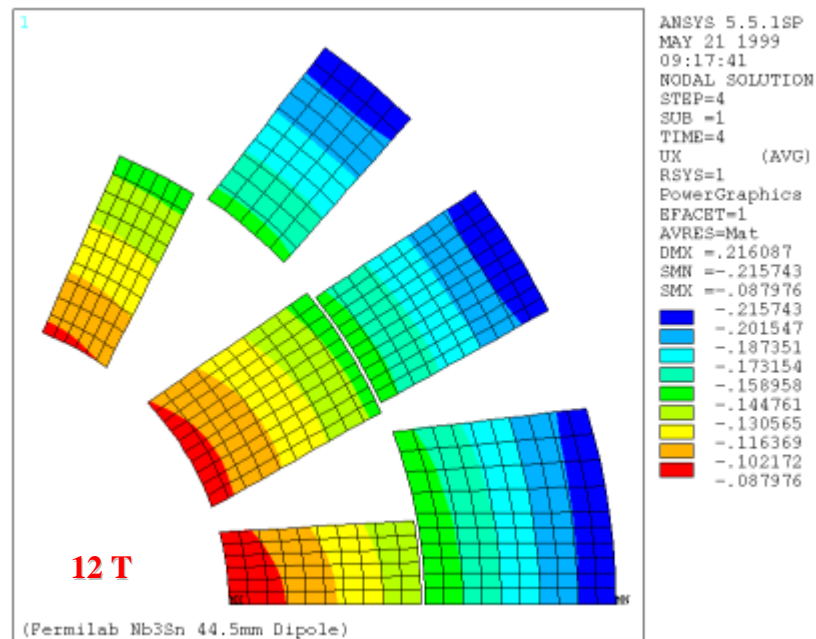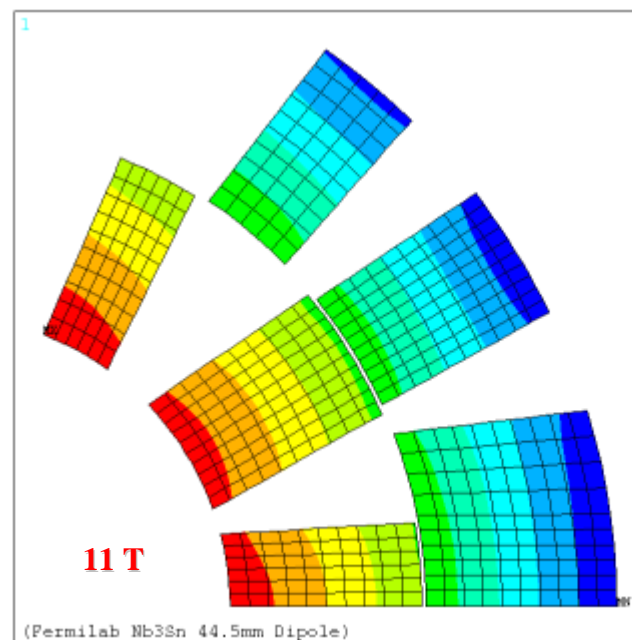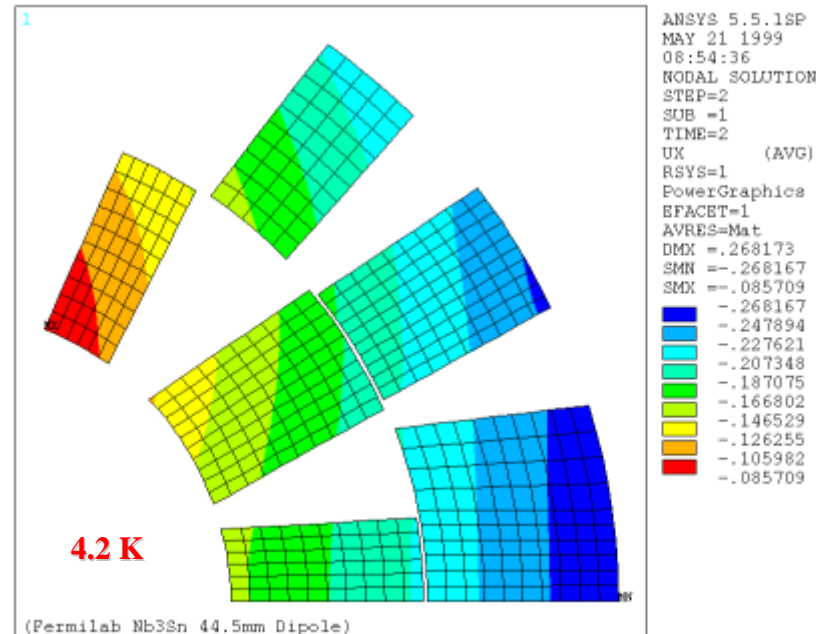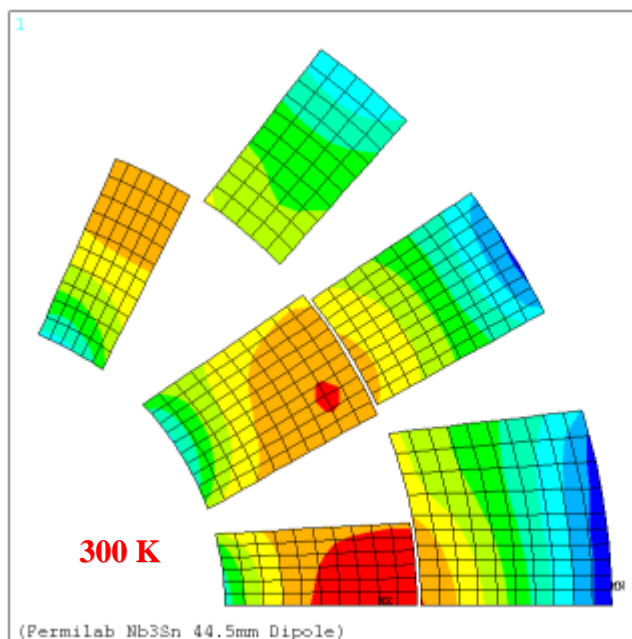**Figure 7**: *Radial displacement contour plots of the coils for CASE 2*

Figure 8: *Azimuthal stress distribution in the coils for CASE 3*
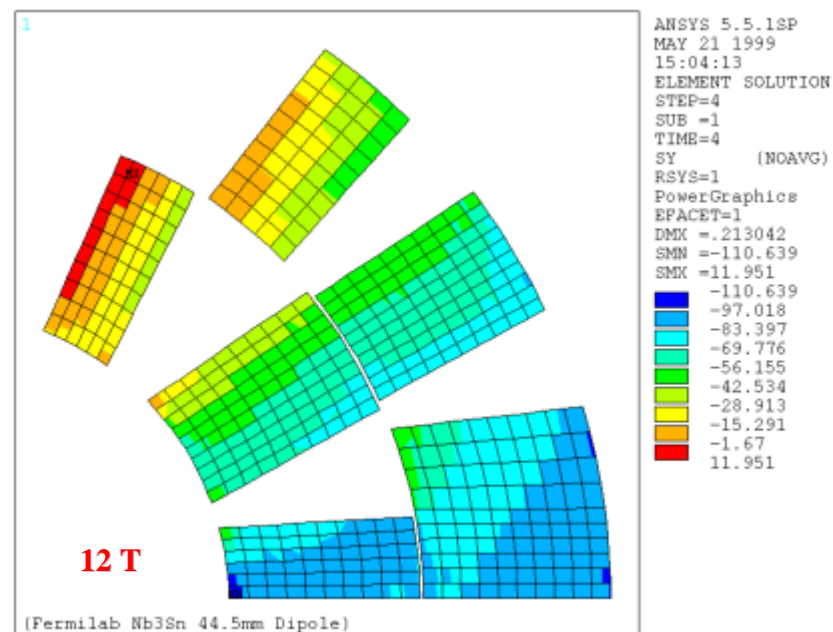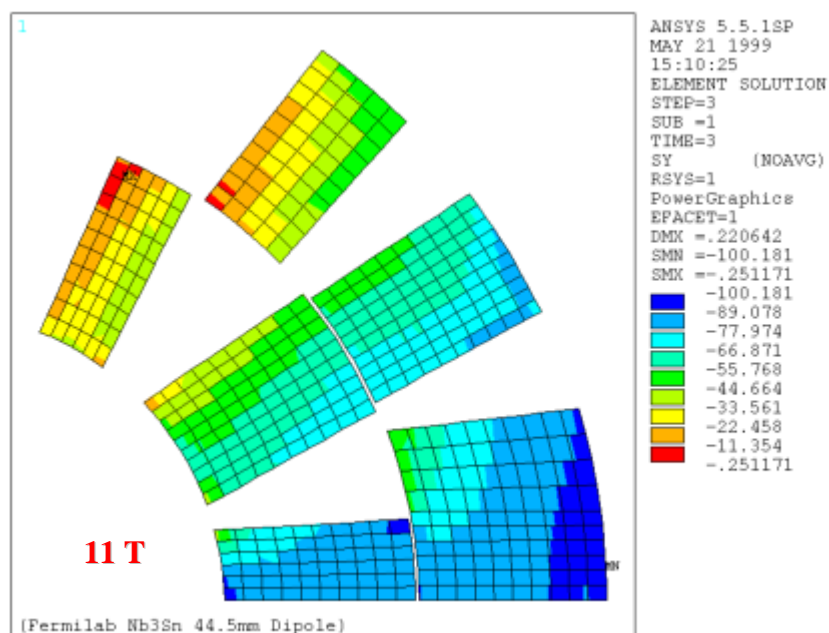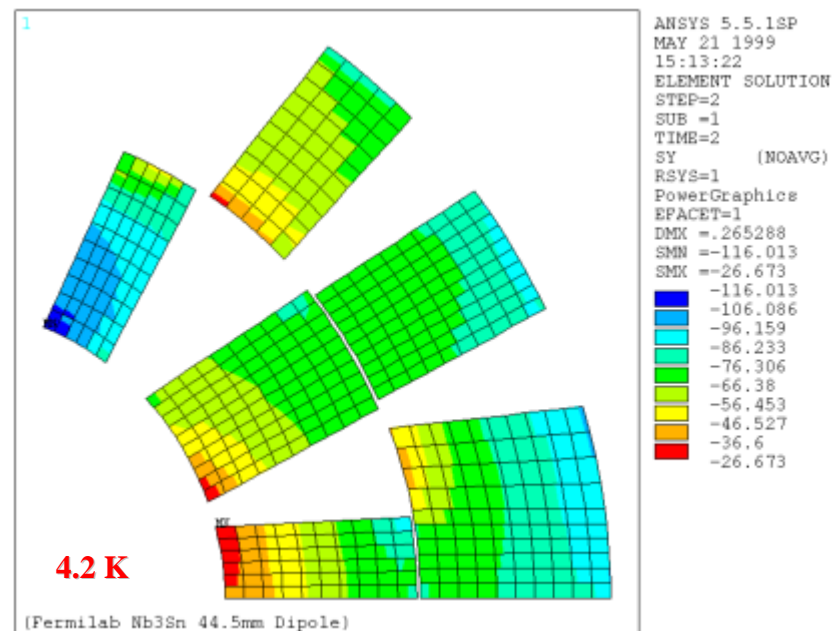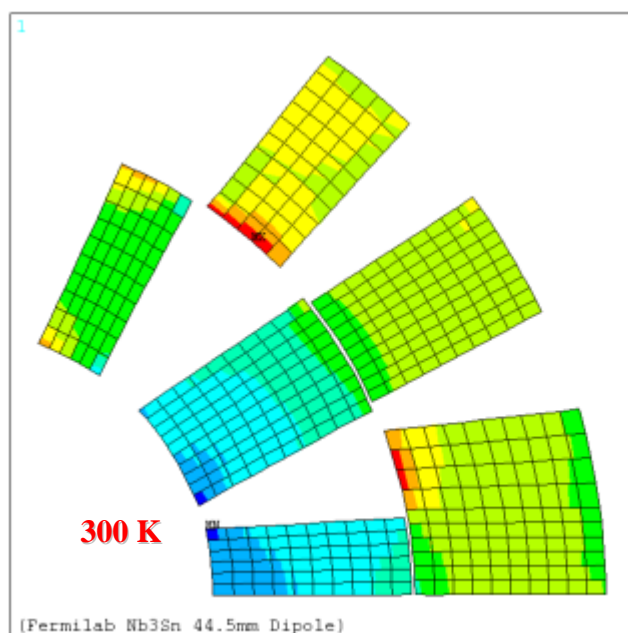
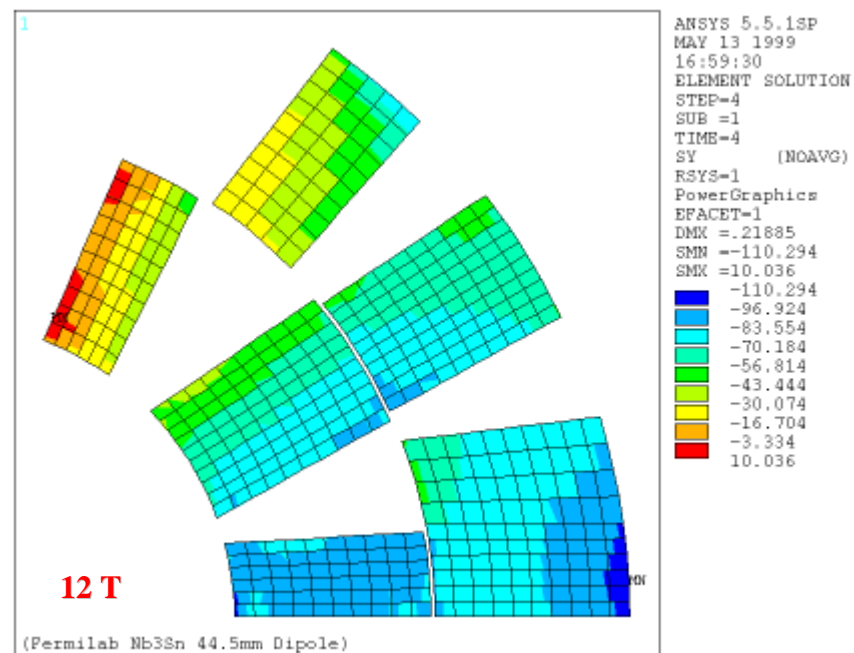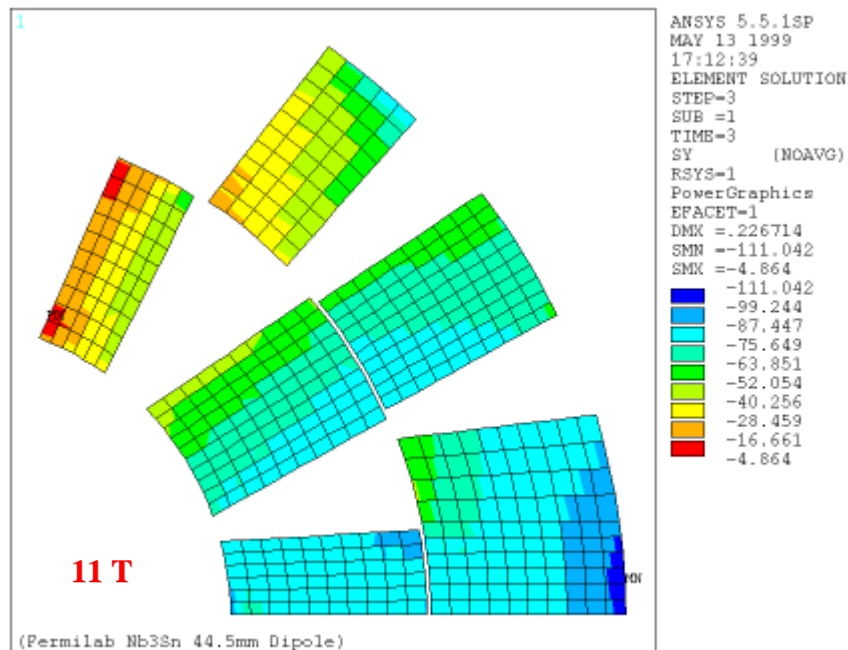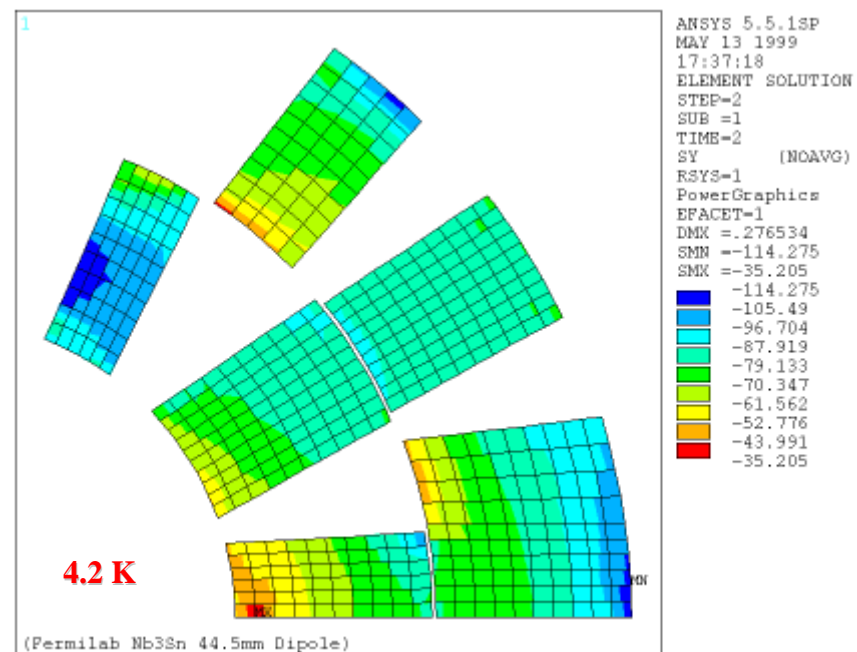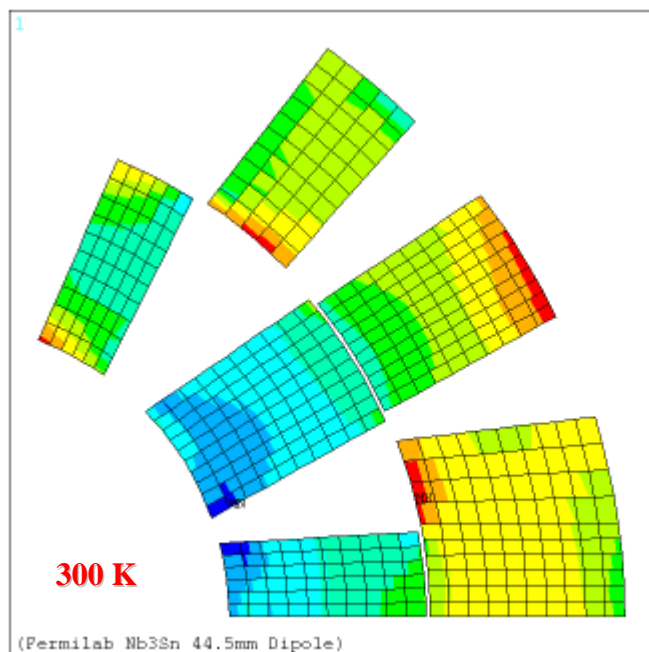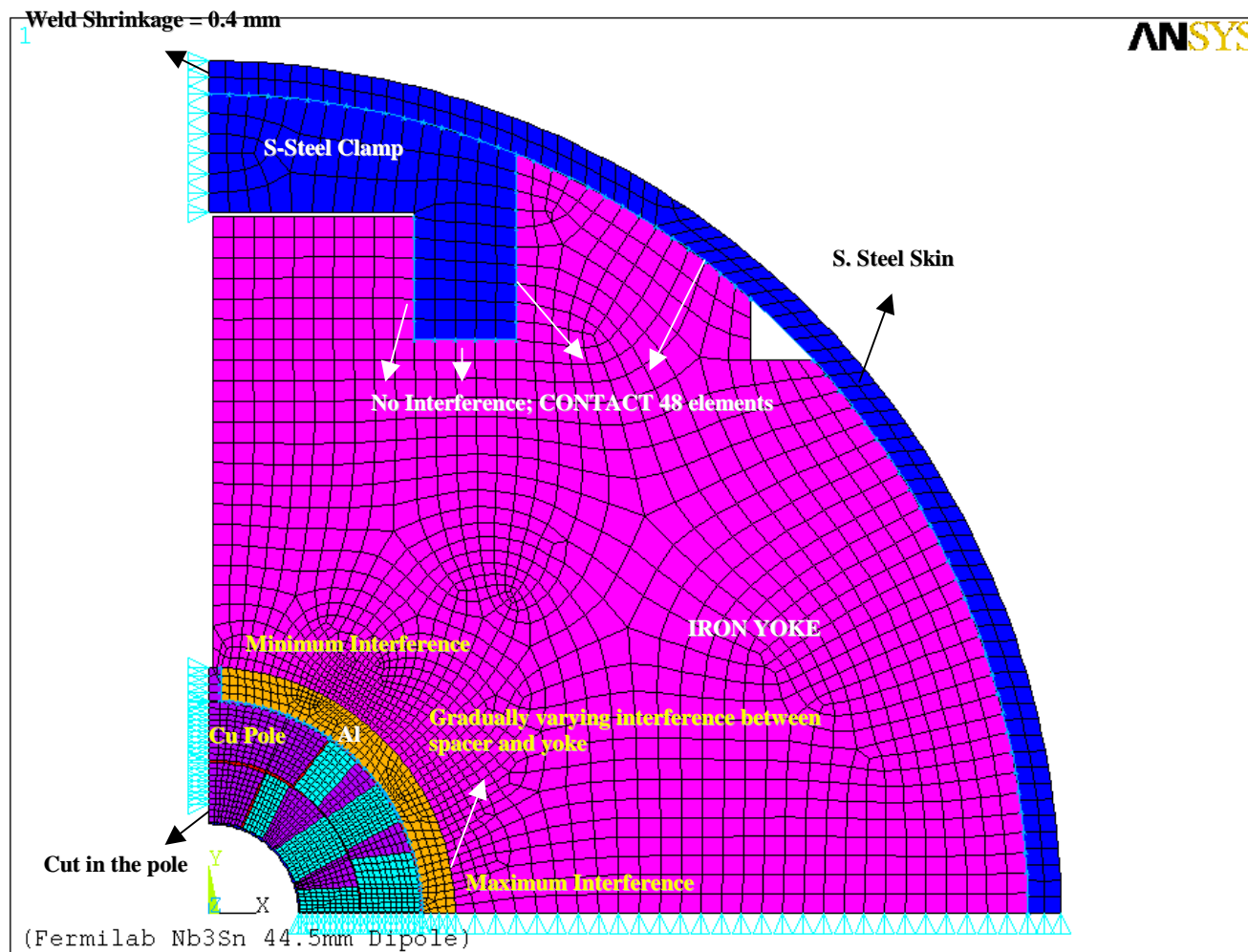**Figure 9**: *Azimuthal stress distribution in the coils for VERSION-2*

Figure 10: *ANSYS model for Version - 2.*

4.0 Mechanical Analysis: VERSION - 2

ANSYS model for Version - 2 is shown in Fig. 10. In this version there is neither azimuthal interference between the spacer and the pole extension nor interference between clamp and the yoke; instead we have a gradually varying radial interference between the spacer and the yoke. The maximum interference (= 225 µm) is at the midplane and minimum (=100 µm) at the pole. This variation of interference is chosen to compress the coil assembly more in the horizontal direction thus increasing the stress in the pole region. The interference between the clamp and the yoke in version - 1 does the same job. Note that the weld shrinkage provides pre-stress to the coil assembly through radial compression. For a constant radial interference between the spacer and the yoke, the difference in stress levels in the mid-plane and the pole region is quite large with maximum at the mid-plane and minimum at the pole region. The increase in the stress in the pole-region after cool-down is then not sufficient to hold the coil assembly in compression during excitation.

The idea behind this version is to eliminate tighter tolerances on clamp dimensions. Magnet mechanics will remain the same as in Version - 1. The azimuthal stress distribution in the coils is shown in Fig. 9. Table 5 summarizes the stress distribution in the magnet. The peak stress in the coil is around 115 MPa during cooldown at the pole region. Note that the location of the maximum stress is radially shifted due to the cut in the pole insert. The major difference between the version - 1 and version -2 is the radial deformation in the coil assembly. In version - 1, there is no difference in the radii at pole and mid-plane at room temperature and during excitation. However after cooldown, the mid-plane moves radially inwards more than the pole region by 80 µm. In this version, mid-plane and pole region deform differently at all stages of the magnet. The maximum deformation from cooldown until peak field is 127 µm which is acceptable.

	Azimuthal Stress, MPa				
	300 K	4.2 K	11 T	12 T	
COIL					
Position 1	63	114	5	-10	
Position 2	110	44	87	96	
Position 3	83	87	52	56	
Position 4	90	105	111	110	
σ**(max)**	108	115	115	118	= von-mises
SPACER	115	80	40	30	= σ(azimuthal)
CLAMP	-218	-115	-174	-180	= σ(x)
δR	20	-80	30	47	**= R(mid-plane)-R(pole),** µm

Table 4: *Stress values in the coil assembly, spacer and clamp for Version - 2.*

5.0 <u>Summary</u>

Mechanical analysis of the 44.5 mm bore dipole magnet for two different versions has been presented. In version - 1, the coil pre-stress at room temperature is provided by the interference between the yoke and the clamp and weld-shrinkage, where as in version - 2, a gradually varying radial interference between the spacer and the yoke along with weld shrinkage provide the necessary pre-stress for the coils. For version - 1, CASE - 3 (spacer and clamp made out of aluminum) might be a likely choice for the final dipole as the room temperature stress in the coil assembly is lower than that in CASE - 2 (spacer with aluminum and clamp is stainless steel). Between version - 1 and version - 2 the decision will be made after performing sensitivity analysis on each variation.

NOTE: The first dipole magnet at Fermilab will be 43.5 mm bore. The reason for this change was that the insulation thickness increased from 5 to 10 mils and the outer radius of the coil assembly had to kept the same to use the present LHC IR Quad tooling. The mechanical analysis and the sensitivity analysis for both the versions will be performed for this design which will be reported in a later technical note.